Case Studies in Thermal Engineering 28 (2021) 101671

Contents lists available at ScienceDirect

Case Studies in Thermal Engineering

journal homepage: www.elsevier.com/locate/csite

Productivity forecasting of solar distiller integrated with evacuated tubes and external condenser using artificial intelligence model and moth-flame optimizer

Ammar H. Elsheikh [c,*], Hitesh Panchal [b], Mahmoud Ahmadein [a,c], Ahmed O. Mosleh [d], Kishor Kumar Sadasivuni [e], Naser A. Alsaleh [a]

[a] Mechanical Engineering Department, Imam Mohammad Ibn Saud Islamic University, Saudi Arabia
[b] Mechanical Engineering Department, Government Engineering College Patan, Gujarat, India
[c] Production Engineering and Mechanical Design Department, Faculty of Engineering, Tanta University, Tanta, Egypt
[d] Shoubra Faculty of Engineering, Benha University, Shoubra St. 108, Shoubra, P.O. 11629, Cairo, Egypt
[e] Centre for Advanced Materials, Qatar University, Qatar

ARTICLE INFO

Keywords:
Solar distiller
Evacuated tubes
External condenser
Forecasting
Moth-flame optimizer
LSTM neural Network

ABSTRACT

This paper aims at developing an artificial intelligence model to forecast the water yield of a modified solar distiller integrated with evacuated tubes and an external condenser. The model consists of a hybrid long short-term memory (LSTM) model optimized by a moth-flame optimizer (MFO) used as a subroutine to obtain the optimal internal parameters of the LSTM model that maximize the forecasting accuracy. The model performance was compared with that of the standalone LSTM model. Both developed models were trained and tested using experimental data of the modified distiller and a conventional distiller. The thermal performance of both distillers is also compared in this article. The maximum daily distillate output achieved for the modified distiller was 3920 l/m^2. The forecasted data of both models were compared using several statistical measures. For all measurements, LSTM-MFO outperformed standalone LSTM. The determination coefficient of the forecasted data using LSTM-MFO reached a high value of 0.999 for both solar distillers.

1. Introduction

With the rapid growth of the world population and aggravated industrial development, the freshwater shortage has become a significant world crisis and human challenge [1]. Only 3% of the water on the earth can be used for domestic and industrial purposes, and the remaining amount is saline water [63]. Seawater desalination can help to provide the coastal cities with freshwater [62]. Both fossil fuels and renewable energy sources are used to operate seawater desalination systems. However, desalination systems powered by fossil fuel sources produce greenhouse gas emissions which cause a significant increase in air pollution. Hence, renewable energy sources such as solar energy and geothermal energy are highly recommended for seawater desalination systems [2].

Solar distillers are eco-friendly desalination units used in seawater desalination and powered by solar energy. They have a simple structure fabricated using a simple manufacturing process [64–66]. Nevertheless, they suffer from low distilled water productivity and low efficiency [3]. A lot of research has been conducted for improving the efficiency of solar distillers by modifying their design such as

* Corresponding author. Ammar Elsheikh
E-mail address: ammar_elsheikh@f-eng.tanta.edu.eg (A.H. Elsheikh).

https://doi.org/10.1016/j.csite.2021.101671
Received 19 June 2021; Received in revised form 14 November 2021; Accepted 23 November 2021
Available online 27 November 2021

single slope distiller [4], single basin distiller [5], tubular distiller [6], double slope distiller [7], distillers with glass cooling [8], double basin distiller [9], solar distillers with nanofluids and phase change materials [10–12], stepped distiller, pyramid distiller [13], and fins [14]. Furthermore, integrations between solar distillers and different engineering system like evacuated tubes with fins [15], evacuated tube collector [16], ultrasonic vaporizer [17], photovoltaic modules [18], parabolic trough solar collector [19], external condenser [20], heat pipe solar collector [21], solar chimney [22], flat plate collector [23], solar water heater [24], and Fresnel lens [25] have been reported.

Morad et al. [26] experimentally investigated the performance of a conventional solar distiller connected to a traditional solar collector with a flat-plate absorber. The distiller produced a high distilled water productivity of 10.06 l l/m^2.day when the glass cover was cooled down using the flash cooling technique. Abu-Arabi et al. [27] developed a compound desalination unit comprised of a solar distiller, with steel pipes filled with sodium thiosulfate pentahydrate, paraffin wax, or sodium acetate trihydrate in the basin and a glass cooling, connected to an external collector. The use of an external collector helps in providing additional heat to the water basin, which enhances the system's productivity of 7.4 ml/min was achieved for the hybrid system. Al-harahsheh et al. [28] established a solar distiller containing a copper tube filled with phase change material and integrated with an external solar collector. The distilled water productivity of the distiller was 4.3 l/day.m^2. The solar collector enhances the distilled water productivity of the system by providing the system with continuous energy, which improves the performance of the energy storage device and consequently enhances the system's productivity at night. A compound desalination unit comprised of a solar distiller and a parabolic trough collector has been developed by Amiri et al. [29]. The established system produces more freshwater in summer than in winter by about 55% for parabolic troughs with a fixed structure. It reaches 70% if the parabolic trough is connected to a tracking system. A double slope solar distiller integrated with a parabolic concentrator, a photovoltaic module, and a coiled heat exchanger was experimentally investigated by Arora et al. [30]. The water productivity of the investigated system was augmented by about 65.7% compared with that of a standalone solar distiller. A single slope solar distiller equipped with a solar air collector, an external condenser, a spraying unit, and a flat plate solar collector was developed by Eltawil and Omara [31]. The daily freshwater productivity of the developed hybrid system is improved by about 142% compared to a standalone solar distiller. Sadeghi and Nazari [32] established a hybrid desalination unit comprised of a single slope solar distiller, an evacuated tube collector, and a thermoelectric-equipped channel. Compared with a standalone solar distiller, the established system ameliorates the energy efficiency and daily distilled water productivity by 117% and 218%. The integration between a passive single-slope solar distiller and an external condenser enhanced the water productivity of the system by 92.3% [33]. The integration between an active solar distiller, an evacuated tube solar collector, and a condenser enhanced the water productivity of the system by 66% [34].

Modeling hybrid solar desalination systems is a cumbersome problem requiring advanced modeling techniques such as artificial intelligence to avoid solving complex mathematical models [35]. Mashaly et al. [36] employed an artificial neural network (ANN) approach to model the thermal behavior of solar distiller for different waters. A neuro-fuzzy inference system (ANFIS) model was used to predict a double-slope tubular solar distiller [37]. In another study [38], the same research group utilized an ensemble random vector functional link model to estimate the distilled water productivity of an active solar distiller integrated with an exterior condenser. Santos et al. [39] used local weather data to train the ANN model employed to predict the distilled water productivity of commercial solar distillers. Elsheikh et al. [40] developed long short-term memory (LSTM) neural network model to forecast the water productivity of a stepped solar distiller. The developed model outperformed the traditional autoregressive moving average technique according to the statistical evaluation of the forecasted data. Nevertheless, the traditional artificial intelligence models suffer from some inherent problems, such as trapping into local minima. Moreover, selecting the optimal structure and the model's internal parameters is another critical issue that should be investigated to enhance the model's prediction capability.

Metaheuristic optimizers [41–43] have been proposed as efficient subroutines that optimize the performance of different artificial intelligence predictive models. From literature, numerous metaheuristic optimizers have been used to fine-tuned the artificial intelligence models for different engineering problems such as gradient-based optimizer [44], Hunger games optimizer [45], pigeon optimizer [46], equilibrium optimizer [47], manta ray foraging optimizer [48], political optimizer [49], parasitism-predation algorithm [50], ecosystem-based optimizer [51], flower pollination optimizer [52], and equilibrium optimizer [53].

Essa et al. [54] developed a compound artificial intelligence model to forecast the distilled water productivity of an active solar distiller connected to an exterior condenser. The model is composed of an ANN model fine-tuned using a metaheuristic optimizer called Harris hawks optimizer. The predicted data using the proposed hybrid model had a high correlation coefficient of 0.922 with the target data. Bahiraei et al. [55] employed a particle swarm optimizer to optimize ANFIS and ANN models to predict the performance of solar distiller integrated with thermoelectric modules. The correlation coefficient increased 0.9508 to 0.9904 for the predicted data of ANN and the optimized ANN, respectively.

In this study, two single-basin single-slope solar distillers are designed, established, and tested under the same meteorological conditions. The second distiller is integrated with an evacuated tube and an external condenser. The performance of both distillers is compared. Furthermore, an advanced artificial intelligence-based model comprised of an LSTM model and moth-flame optimizer is developed to forecast the water productivity of the established solar distillers. The developed model is compared with standalone LSTM using statistical evaluation measures.

2. Experimental methodology

The experiments were conducted in an atmospheric condition of Gandhinagar, Gujarat, India. One conventional solar distiller (CSD) and another modified solar distiller (MSD) was designed and established to compare the performances of the two solar distillers [20]. Both CSD and MSD were made from the same wooden materials, having a basin area of 1 m^2. To absorb the solar irradiance, the

basin surface was painted using black color. The top side of the solar distiller was covered with a transparent glass cover with a thickness of 4 mm. In the modified solar distiller, six evacuated tubes and an air-cooled condenser were attached. Pebbles were added to the basin of the modified distiller and acted as a sensible heat storage material. In Fig. 1, the schematic and pictorial views of both solar distillers are shown. An evacuated was attached to preheat the saline water inside the solar distiller basin, which increases the evaporative heat storage capacity of a solar distiller. A condenser was used to maintain the inner vapor pressure of the solar distiller and lower the inner glass cover temperature.

All experiments were conducted from 7:00 a.m. of a day to 6:00 a.m. of the next day for all working days in the climatic conditions of Gandhinagar city. In both conventional and modified one solar distiller, water levels were kept constant, having 3 cm. A water level indicator was used, which maintains the constant water level in both solar distillers from overhead water tank constant water supplied to both distillers. With increasing solar intensity, water inside the solar distiller gets heated. Also, an evacuated tube preheats the water inside a modified solar distiller, which increases its basin water temperature and evaporative heat capacity. The more vapor generated inside the modified solar distiller moves towards the condensation area where it condenses. The freshwater could be collected from the

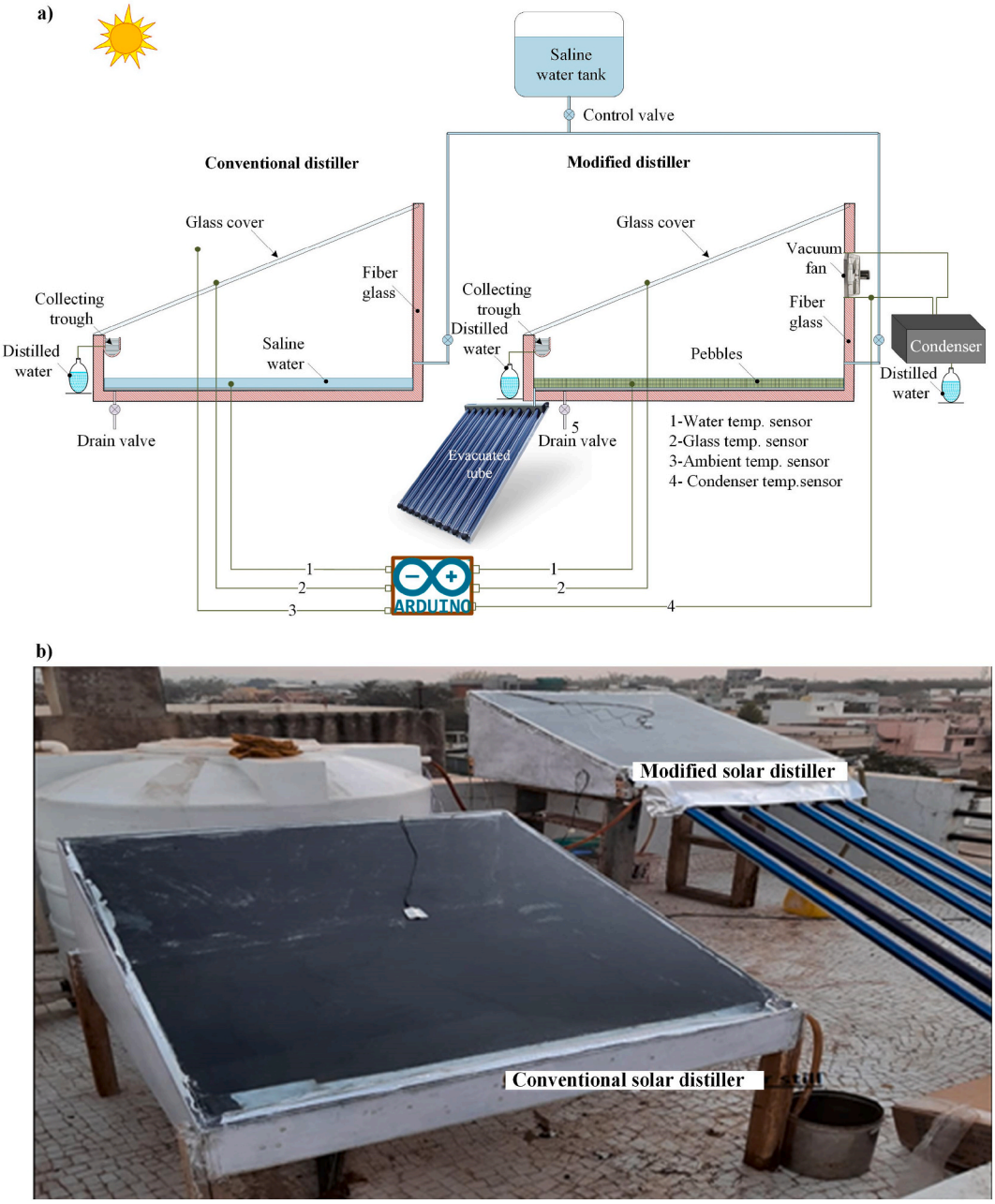

Fig. 1. The experimental setup: a) Schematic, b) Photo [20].

front and condenser areas in a modified solar distiller. During the experimental work, various operating parameters like ambient temperature (Ta), solar irradiance (I), water temperature (Tw), and inner glass cover temperature (Tgi) were measured and recorded for all working days. The temperature was measured using a k-type thermocouple sensor. A solarimeter was used to measure the solar intensity. A data logger was used to record all of the experimental readings.

3. Artificial intelligence modeling

3.1. Long-short-term memory network

Artificial neural networks (ANNs) have been widely used in predicting and forecasting the responses of different engineering processes [56,57]. Long-short-term memory (LSTM) is an advanced, recurrent ANN model which has shown promising applications in the deep learning and forecasting field [58]. LSTM can recall old patterns and remember them for a long time due to its innovative structure composed of multiple feedback connections. This innovative structure gives LSTM a significant advantage over traditional feed-forward ANN. LSTM avoids the vanishing/explosion gradient problem, which is a severe problem of recurrent ANN models via varying the self-loop weights by adding input, forgetting, and output gates. Furthermore, LSTM has outstanding advantages for forecasting the future behavior of time-series data with nonlinear nature [58]. The network arrangement of an LSTM model is presented in Fig. 2.

An LSTM unit is composed of three gates and a memory cell. The cell state is considered the core of the unit. It could be represented as a conveyor belt that moves through the memory cell carrying the information. The cell state is regulated using input, forgetting, and output gates. It is composed of point-wise multiplication operators, tanh and sigmoid activation functions. The sigmoid function has a regulated output ranging between 0 and 1. If its value is equal to zero, then no information can pass through the unit. If its value is equal to unity, then all information can pass through the unit.

The forget gate acts as a decision-making unit to determine the trivial information that should be omitted from the cell state. This gate comprises a cell state D_{t-1}, hidden layer f_{t-1}, and an input X_t. The outputs of D_{t-1} range between 0 and 1. The forget gate is mathematically represented as follows:

$$f_t = S(W_h f_{t-1} + U_i x_t + b_h) \tag{1}$$

The input gate acts as a decision-making unit to determine the information that can be preserved in the cell state. Closing the input gate means that all information is prevented from transmission to the memory cell. This distinctive function helps the memory cell to preserve data for the following updating process. Two activation functions are used to process the information in this gate, namely sigmoid, which is used to select the updated information I_t, and a tanh function creates a new vector $\widehat{D}_t$. The input gate converts the old state D_{t-1} into a newly updated stateD_t.

$$I_t = S(U_i x_t + W_i f_{t-1} + b_i) \tag{2}$$

$$\widehat{D}_t = T\left(U_{\widehat{c}} x_t + W_{\widehat{c}} f_{t-1} + b_{\widehat{c}}\right) \tag{3}$$

$$D_t = I_t \odot \widehat{D}_t + f_t \odot D_{t-1} \tag{4}$$

The output gate produces the information that flows through the next cell state.

$$O_t = S(U_o x_t + W_o f_{t-1} + b_o) \tag{5}$$

Finally, the new state is computed as follows:

$$\mathbb{Z} = T(c_t) \odot O_t \tag{6}$$

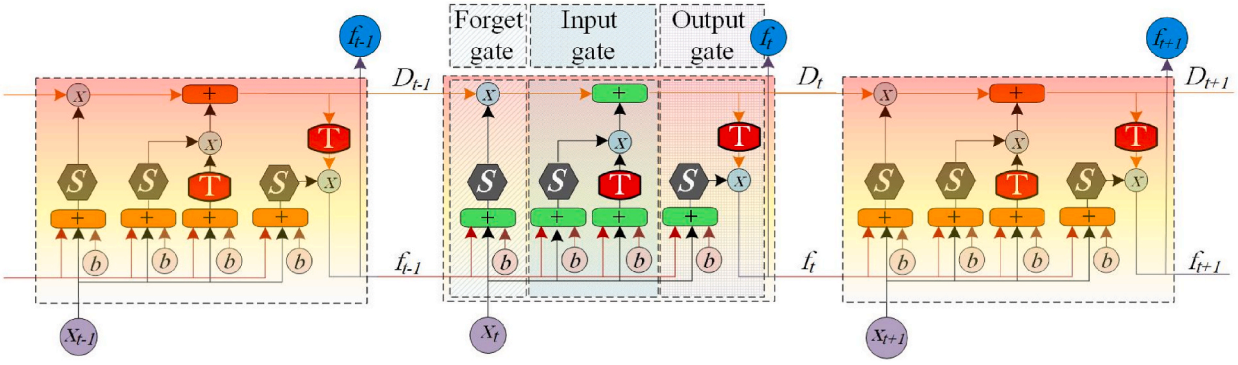

Fig. 2. The network arrangement of an LSTM model [59].

where D_t, $\widehat{D}_t$ $\mathbb{Z}$, and O_t are cell sate, potential cell state, hidden state, and output gate, respectively; $T(\cdot)$ denotes the hyperbolic tangent activation function; $S(\cdot)$ denotes an activation function called sigmoid, (b, W, U) are the bias/weight at the gates.

3.2. Moth-flame optimizer

Moth-flame optimizer (MFO) is a nature-inspired optimizer that mimics the natural navigation behavior of moths fly [60]. These flies maintain a constant angle with the moon during nighttime e and apply an intelligent technique during traveling for long distances. Nevertheless, these flies are trapped in a deadly/useless path with a spiral shape when they watch any artificial lights. To model this behavior using mathematical tools (X_i, $i = 1, 2, \ldots, Z$). The positions of moths represent the model parameters, and the optimal position of these moths is considered a flame. The algorithm of MFO contains random population (R), moving function (M) that describes the navigation of moths in the search space, and the model parameters (P) that are used to terminate the optimization process. The algorithm is given as a function of the parameters mentioned above:

$$MFO = (R, M, P) \tag{7}$$

In the moving function M, the positions of moths are reorganized based on the flames using the following equation:

$$A_i = \mathscr{S}(A_i, B_j) = C_i \cdot e^{br} \cdot cos(2\pi t) + B_j \tag{8}$$

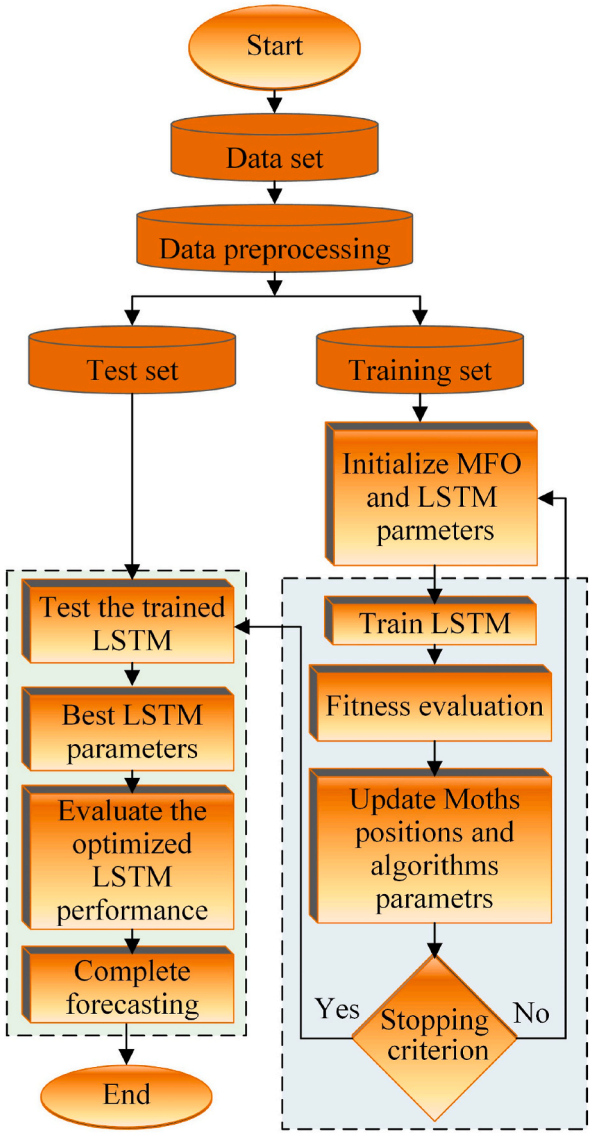

Fig. 3. The execution procedures of the proposed LSTM-MFO model.

where $\mathscr{S}$, B_j, and A_i represent the spiral function. jth flame and ith moth, respectively. C_i denotes the distance between the jth flame and ith moth. b denotes a constant used to define the spiral geometry. r is a randomly generated number in the range [-1, 1]. The distance C_i is computed as follows:

$$C_i = \left|B_j - A_i\right| \tag{9}$$

The exploration phase of the search space is maintained following an adaptive strategy to reduce the number of flames as follows:

$$N = round\left(N_{max} - \alpha \times \frac{N_{max} - 1}{\xi}\right) \tag{10}$$

where N, N_{max} , ξ, and α represent the number of flames, total number of flames, total number of iterations, and the current iteration number, respectively.

3.3. Optimized model

To optimize the performance of LSTM, MFO is used as a subroutine to obtain the optimal parameters of LSTM that maximize the forecasting accuracy. The optimized internal parameters of the network are the number of nodes, weights, and the learning rate, respectively. The optimization process is executed via minimizing an objective function. This objective function is an error measure defines the deviation between the forecasted and target data. Herein, root-mean-square deviation RMSD is used as an objective function:

$$RMSD = \sqrt{\frac{1}{m}\sum_{k=1}^{N}\left(x_k - \widehat{x}_k\right)^2} \tag{11}$$

where m, x_k , and x_k denote the number of training data, the value of the target data, and the value of the forecasted data, respectively.

The execution procedures of the proposed LSTM-MFO model are presented in Fig. 3. The training data is preprocessed and divided into two groups, test set, and training set. The parameters of LSTM and MFO are initialized. Then, the LSTM network is trained using the training set, and the fitness function is evaluated. The model parameters are updated to minimize the fitness function until the stopping criterion is achieved. Once the stopping criterion is reached, The LSTM with the optimal parameters is tested. Various statistical criteria assess its performance. Finally, the optimized LSTM network is employed to forecast the distilled water productivity of the solar distillers.

3.4. Model evaluation criteria

The accuracy of LSTM and LSTM-MFO models has evaluated the statistical measures tabulated in Table 1 [61].

4. Results and discussions

4.1. Experimental evaluation

In Fig. 4 (a), hourly variations of ambient temperature with time for all working days are shown. Atmospheric temperature is an essential parameter for an experimental result. Atmospheric temperature is varied with solar intensity. With higher solar intensity, a higher ambient temperature could be achieved. The slope of ambient temperature for all days is relevant to each other, so it means not measure variation in temperature differences could be achieved during experimental work. The highest ambient temperature was reached is 42.50 °C at 15:00 p.m.; because of the maximum solar irradiance at this time. In the noontime, the maximum temperature was achieved for all days. In evening hours, the slope for temperature decreases due to lower solar intensity at evening hours. Higher

Table 1
Statistical measures used to evaluate the accuracy of the LSTM and LSTM-MFO models.

Measure	Abbreviation	Formula
Determination coefficient	R^2	$R^2 = \frac{\left(\sum_{i=1}^{m}(x_i-\overline{x})(y_i-\overline{y})\right)^2}{\sum_{i=1}^{m}(x_i-\overline{x})^2 \times \sum_{i=1}^{m}(y_i-\overline{y})^2}$
Mean absolute error	MAE	$MAE = \frac{1}{m}\sum_{i=1}^{m}\left\|x_i - y_i\right\|$
Mean relative error	MRE	$MRE = \frac{1}{n_s}\sum_{i=1}^{n_s}\frac{d_i - y_i}{d_i}$
Root mean square error.	RMSE	$RMSE = \sqrt{\frac{1}{m}\sum_{i=1}^{m}(x_i - y_i)^2}$
Efficiency coefficient	EC	$EC = 1 - \frac{\sum_{i=1}^{m}(x_i - y_i)^2}{\sum_{i=1}^{m}(x_i - \overline{y})^2}$
Overall index	OI	$OI = \frac{1}{2}\left(1 - \left(\frac{RMSE}{x_{max} - x_{min}}\right) + EC\right)$
Coefficient of variation	COV	$COV = \frac{RMSE}{\overline{x}} \times 100$

Where *m, x, and y* denote the number of experimental datasets, measured data, and forecasted data. Additionally, $x_{\max}$ and $x_{\min}$ represent the maximum and minimum values of the experimental data, respectively, while $\overline{y}$ and $\overline{x}$ denote mean values of the forecasted and experimental data, respectively.

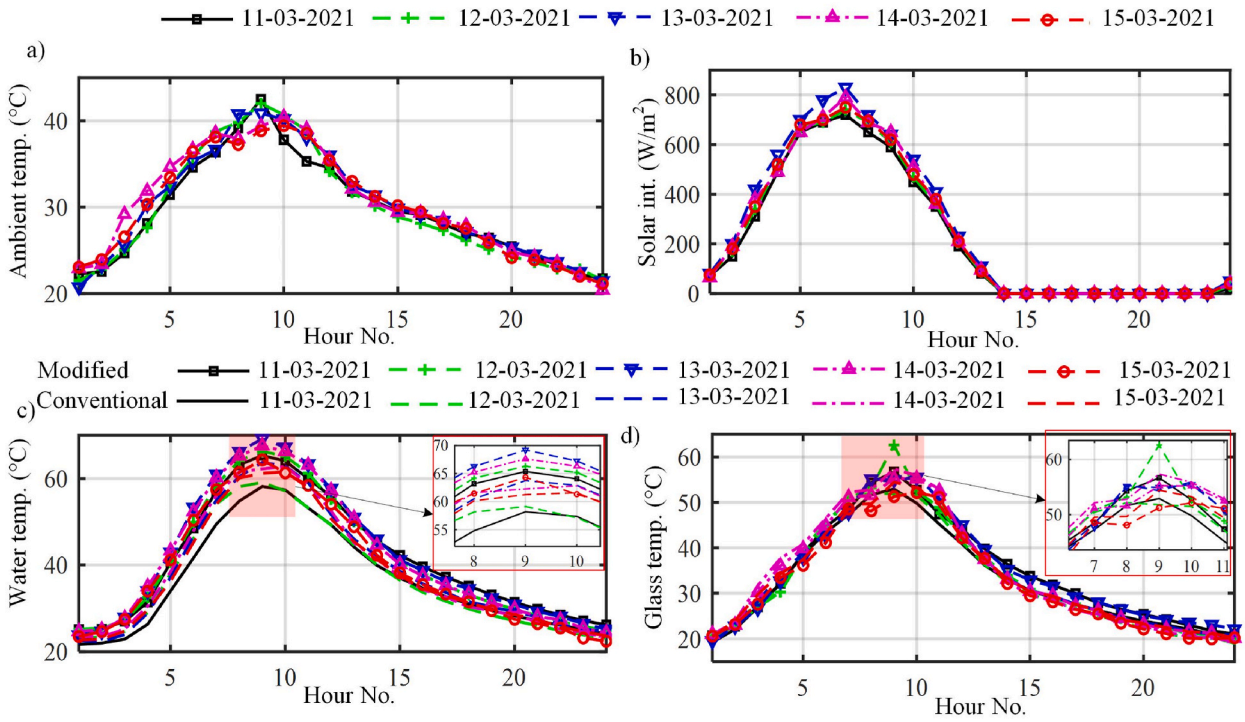

Fig. 4. Variations of: a) ambient temperature; b) solar irradiance; c) water temperature; d) glass temperature.

ambient temperature increases the water temperature of the basin, which enhances the distillate output of the solar distiller.

Fig. 4 (b) shows the hourly variations of solar intensity with time for all working days. Here seven days of experimental readings are taken. In the morning and evening hours, the solar intensity remains lower. So during these hours, lower ambient temperature could be achieved. The figure shows that after 11:00 a.m., solar irradiance increases and reaches its peak value at 14:00 p.m. At this time, a higher basin water temperature may be obtained. The maximum solar intensity that could be achieved was 830 W/m^2 at 13:00 p.m. The higher value of solar irradiance increases the distillate output of the solar distiller. In night hours, due to the absence of solar intensity, the distillate output becomes lower, which lowers the efficiency of a solar distiller.

Higher the basin water temperature increases the distillate productivity of solar distiller. Fig. 4 (c) shows the hourly variations of basin water temperature for conventional solar distiller (CSD). In a conventional solar distiller, the basin water temperature is varied with time. In the morning hours, the temperature becomes lower due to lower ambient temperature and solar intensity. In the afternoon time, a higher water temperature may be obtained. The maximum water temperature achieved for conventional solar distiller was 63.75 °C at 15:00 p.m. The water temperature in CSD remains lower compared to modified solar distiller (MSD). It happens due to the existence of evacuated tubes and condensers in a modified solar distiller. The lower water temperature could be achieved during the evening hours because of lower solar intensity in the sky. It also decreases the nocturnal productivity of solar distiller.

In Fig. 4 (c), an hourly variation of basin water temperature for modified solar distiller is also shown. Six evacuated tubes were connected to the modified solar distiller to achieve a higher water temperature and preheat the saline water inside the basin area. The maximum saline water temperature achieved for MSD and CSD was 69.21 °C and 63.75 °C, respectively, at 15:00 p.m. In MSD, water temperature is higher than that of CSD by about 6 °C. Thanks to the use of evacuated tubes with MSD, the higher basin water temperature could be reached; it also increases the evaporative heat transfer coefficient of MSD compared to CSD. From the figure, it could be found that the lines of water temperature for all days are varied with each other. The water temperature for the modified solar distiller changed day by day during experimental work. Also, in the night hours, the water temperature in MSD is higher than that of CSD.

Higher inner glass cover temperature increases the top heat losses of a solar distiller, which decreases the distillate productivity and efficiency of a solar distiller. In Fig. 4 (d), variations of inner glass cover temperature for CSD are shown. In CSD, the inner glass cover temperature remains higher compared to MSD. From the figure, it could be found that the inner glass cover temperature shows the maximum for all days during noon hours. The single maximum inner glass cover temperature for CSD was 55.93 °C at 15:00 p.m. The higher inner glass cover temperature decreases the daily distillate productivity of CSD. To increase the productivity of solar distiller, the inner glass cover temperature should be lower. Fig. 4 (d) shows the hourly variations of inner glass cover temperature for a modified solar distiller. The higher water temperature and lowered inner glass cover temperature increase the distillate productivity of solar distiller. In MSD, an air-cooled condenser was attached to maintain this temperature difference, which reduces the temperature of the inner glass cover in MSD. The highest inner glass temperature achieved for MSD was 54.93 °C at 15:00 p.m., which was lower than CSD. In MSD, a higher water temperature could be obtained by preserving the inner glass cover temperature. In an MSD condenser,

decrease the pressure inside the basin area by condensing the excess vapor of the basin surface and lowering the temperature of the glass cover. It also increases the volumetric heat transfer capacity of MSD. During night hours, the excess vapor is released by a condenser. It maintains the basin water temperature higher for MSD compared to CSD.

The higher water temperature and lower inner glass cover temperature decrease the distillate output of the solar distiller. To increase the distillate output, this temperature difference should be minimal. In Fig. 5, hourly variations of cumulative distillate output for conventional solar distiller are shown. From the figure, it can be found that distillate output is continuously increased. The maximum total distillate output achieved for CSD was 2430 l/m^2 in a single day. During night time the distillate output of CSD remains lower due to heat losses from the top of the glass cover. The total distillate output of CSD remains lower compared to MSD. In Fig. 5, hourly variations of the total distillate output of MSD for all working days. From the figure, it could be seen that distillate output increases with time. The maximum distillate output achieved for MSD was 3920 l/m^2 in a single day, higher than CSD. In MSD, attachments of evacuated tubes and condensers give more distillate than CSD. Evacuated tubes increase the temperature of basin water and its evaporative heat transfer capacity; also condenser maintains the inner glass cover temperature of MSD. The higher water temperature and lower glass cover temperature achieved in MSD increase its day and night performance. In MSD, the condenser stores the excess heat during the daytime and performs better during night hours; hence nocturnal distillate output could be increased. Compared to CSD, MSD provides higher nocturnal productivity.

4.2. Forecasting of distilled water productivity

Distilled water productivity of the CSD and MSD was forecasted using two developed models, namely LSTM and LSTM-MFO. The experimental data of the distilled water productivity of the distillers for five days was used as a time series fed to both models. First, the developed models were trained using the experimental data of five days for both solar distillers. Then the distilled water productivity of one subsequent day was forecasted using the trained models. The models were evaluated using different statistical measures by comparing forecasted data with the experimental ones. Eight statistical measures were computed during the models evaluation. Once the models succeed in forecasting the distilled water productivity during the test stage with an acceptable deviation from the experimental data, they may be utilized to forecast the distilled water productivity of the investigated distillers.

For both investigated distillers, 120 datasets (five days) were used to train the LSTM and LSTM-MFO models, and 24 datasets (one day) were used to test the models. The convergence of the LSTM-MFO is a little bit faster than that of standalone LSTM for both solar distillers, as shown in Fig. 6. In Fig. 7 (a), the blue data points are experimental, and the green data points are forecasted during the teat stage. A reasonable agreement is observed between the green data points and blue ones in the green region and Fig. 7 (c). This agreement encourages us to use the LSTM model to forecast future data points shown in the red region. A better agreement between the experimental and forecasted data is observed in the case of LSTM-MFO, as shown in Fig. 7 (b, d). The error between the forecasted and experimental data in the case of LSTM and LSTM-MFO is demonstrated in Fig. 7(e) and Fig. 7 (f), respectively. The error of LSTM-MFO ranges between −0.010–0.005, which is lower than that of LSTM, which ranges between −0.15 and 0.001. The RMSE of LSTM-MFO (0.0053) is lower than that of LSTM (0.0608). The low error of LSTM-MFO compared with LSTM reveals the role of MFO to optimize LSTM parameters to maximize its accuracy. The same conclusion could be drawn from Fig. 8 for MSD. The accuracy of LSTM-MFO is better than that of standalone LSTM. As shown in Fig. 8(a–d), the forecasted data points are in a better agreement with experimental ones compared with that of LSTM during the test stage shaded in green. The error of LSTM-MFO ranges between −0.075–0.076, which

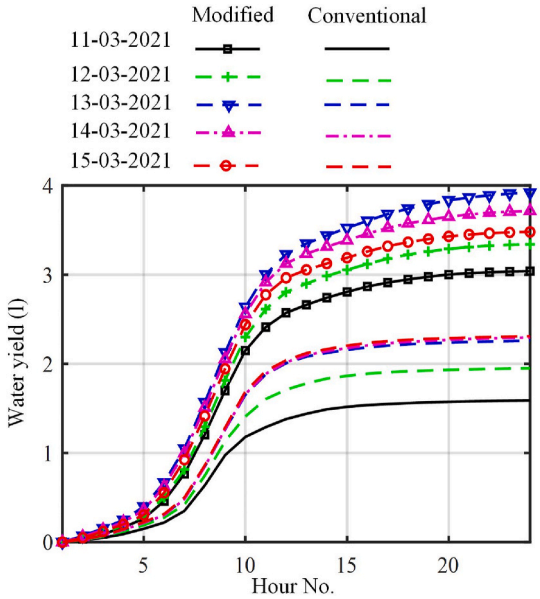

Fig. 5. Variations of accumulated distilled water productivity.

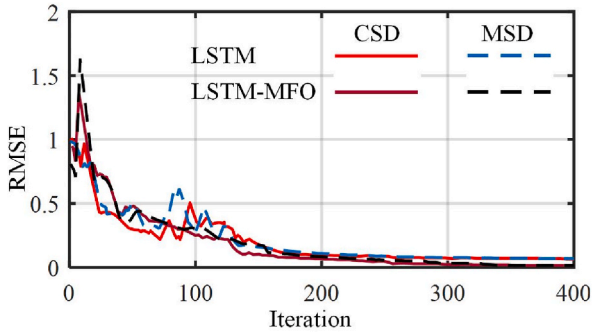

Fig. 6. Convergence curves of LSTM and LSTM-MFO.

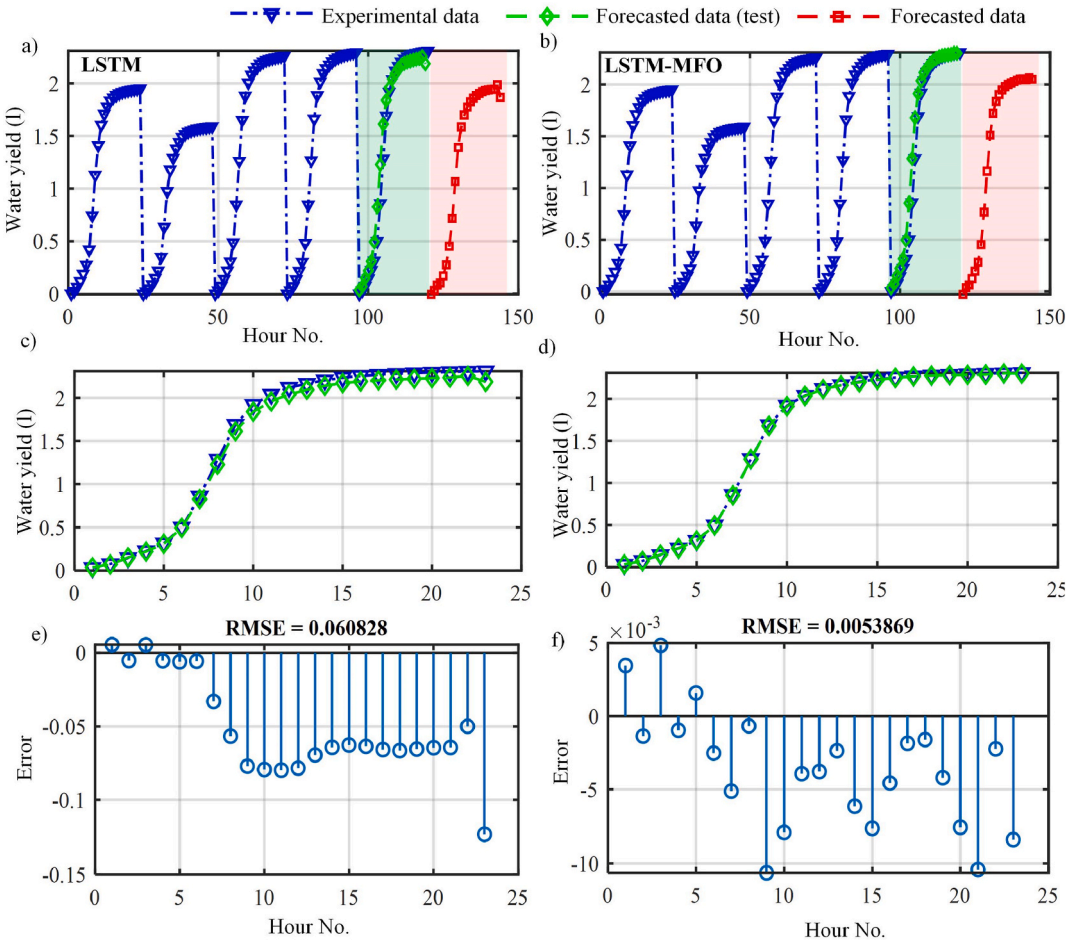

Fig. 7. The forecasted and experimental hourly distilled water productivity for the CSD: a) data series and forecasted yield using LSTM; b) data series and forecasted yield using LSTM-MFO; c) forecasted yield using LSTM in test stage; d) forecasted yield using LSTM-MFO in test stage; e) error of LSTM; f) error of LSTM-MFO.

is lower than that of LSTM, which ranges between −0.1 and 0.12. The RMSE of LSTM-MFO (0.026) is lower than that of LSTM (0.055).

The statistical evaluation of the LSTM and LSTM-MFO models for CSD and MSD using different statistical measures is tabulated in Table 2. LSTM-MFO has a higher R^2, EC, and OI of 0.999, 0.999, and 0.996–0.998, respectively, compared with standalone LSTM, which are 0.997–0.998, 0.997–0.997, and 0.984–0.991, respectively. The higher values of R^2, OI, and EC, which approach the unity, point out the higher performance of the models. Also, it indicates the outperformance of LSTM-MFO compared with standalone LSTM. On the other, LSTM-MFO has lower RMSE, MRE, MAE, COV and CRM of 0.056–0.061, −0.021–0.008, 0.040–0.052, 2.396–4.004, and −0.001 to −0.033, respectively, compared with that of standalone LSTM which are 0.005–0.027, 0.003–0.052, 0.004–0.021, 0.344–1.131, −0.002–0.009, respectively. The lower values of RMSE, MRE, MAE, COV, and CRM, which approach the zero value,

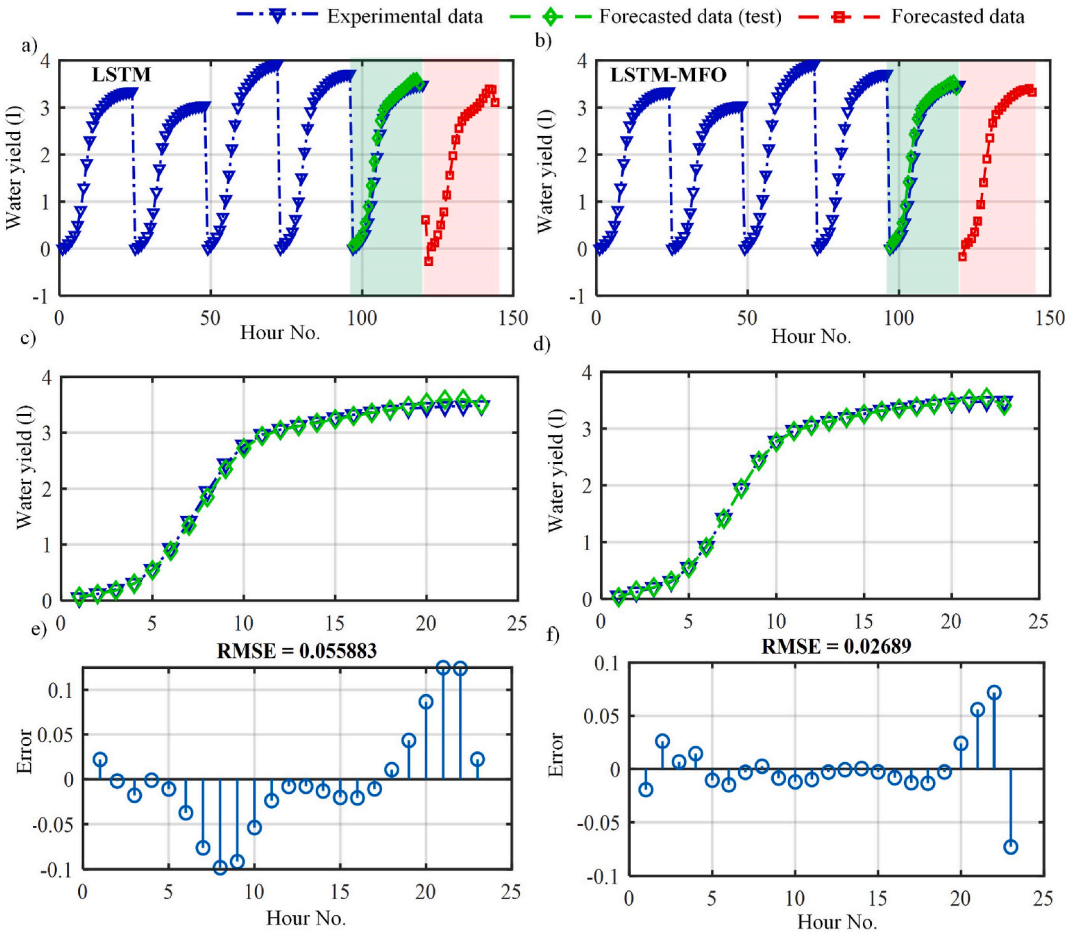

Fig. 8. The forecasted and experimental hourly distilled water productivity for the MSD: a) data series and forecasted yield using LSTM; b) data series and forecasted yield using LSTM-MFO; c) forecasted yield using LSTM in test stage; d) forecasted yield using LSTM-MFO in test stage; e) error of LSTM; f) error of LSTM-MFO.

Table 2
Statistical assessment of the LSTM and LSTM-MFO models.

		R^2	RMSE	MRE	MAE	COV	EC	OI	CRM
CSD	LSTM	0.997	0.061	−0.021	0.052	4.004	0.994	0.984	−0.033
	LSTM-MFO	0.999	0.005	0.003	0.004	0.344	0.999	0.998	−0.002
MSD	LSTM	0.998	0.056	0.008	0.040	2.396	0.997	0.991	−0.001
	LSTM-MFO	0.999	0.027	0.052	0.021	1.131	0.999	0.996	0.009

indicate the higher performance of the models. From an analysis of these measures, it can be declared that LSTM-MFO has a higher accuracy than standalone LSTM to predict the distilled water productivity of CSD and MSD. That is due to the vital role of MFO to determine the optimal model parameters of the LSTM network that maximize the forecasting accuracy. Therefore, LSTM-MFO is suggested to forecast the performance of the investigated solar distillers.

5. Conclusion

This study developed an optimized LSTM model to forecast the freshwater productivity of a standalone single-slope solar distiller and a hybrid solar distiller connected to evacuated tubes and an external condenser. Both solar distillers were established and tested under Indian metrological conditions. The freshwater productivity of the modified solar distiller was improved by 177% compared with that of a standalone solar distiller. The improved freshwater productivity of the modified distiller over the standalone solar distiller is attributed to 1) the role of evacuated tubes to harvest more solar energy; 2) the role of the external condenser to condensate more water vapor. The optimized LSTM model consists of a conventional LSTM model fine-tuned using a moth-flame optimizer. The optimized LSTM outperformed the standalone LSTM due to the vital role of a moth-flame optimizer to find the optimal parameters of the LSTM model that maximize the forecasting accuracy. LSTM-MFO has a higher R^2, EC, and OI of 0.999, 0.999, and 0.996–0.998,

respectively, compared with standalone LSTM, which are 0.997–0.998, 0.997–0.997, and 0.984–0.991, respectively. On the other, LSTM-MFO has lower RMSE, MRE, MAE, COV and CRM of 0.056–0.061, −0.021–0.008, 0.040–0.052, 2.396–4.004, and −0.001 to −0.033, respectively, compared with that of standalone LSTM which are 0.005–0.027, 0.003–0.052, 0.004–0.021, 0.344–1.131, −0.002–0.009, respectively. The higher values of R^2, EC, and OI, which approach the unity, as well as the lower values of RMSE, MRE, MAE, COV, and CRM, which approach the zero value, indicate the higher performance of the optimized LSTM model.

Author statement

Ammar H. Elsheikh: Conceptualization, Methodology, Validation, Formal analysis, Investigation, Writing - original draft, Writing – review & editing; Hitesh Panchal: Conceptualization, Investigation, Resources, Data curation, Writing - review & editing, Supervision, Project administration; Funding acquisition; Mahmoud Ahmadein: Methodology, Data curation, Writing - review & editing. Ahmed O. Mosleh: Conceptualization, Methodology, Writing - review & editing, Supervision, Project administration, Funding acquisition, Kishor Kumar Sadasivuni Methodology, Data curation, Writing - review & editing; Naser A. Alsaleh: Methodology, Data curation, Writing - review & editing;

Declaration of competing interest

The authors declare that they have no known competing financial interests or personal relationships that could have appeared to influence the work reported in this paper.

Acknowledgment

The authors extend their appreciation to the Deanship of Scientific Research at Imam Mohammad Ibn Saud Islamic University for funding this work through Research Group no. RG-21-12-03.

References

[1] A.H. Elsheikh, S.W. Sharshir, M.K. Ahmed Ali, J. Shaibo, E.M.A. Edreis, T. Abdelhamid, et al., Thin film technology for solar steam generation: a new dawn, Solar Energy 177 (2019) 561–575.
[2] A.H. Elsheikh, S.W. Sharshir, M.E. Mostafa, F.A. Essa, M.K. Ahmed Ali, Applications of nanofluids in solar energy: a review of recent advances, Renewable and Sustainable Energy Reviews 82 (2018) 3483–3502.
[3] S.W. Sharshir, A.H. Elsheikh, G. Peng, N. Yang, M.O.A. El-Samadony, A.E. Kabeel, Thermal performance and exergy analysis of solar stills – a review, Renewable and Sustainable Energy Reviews 73 (2017) 521–544.
[4] F.A. Essa, A.H. Elsheikh, A.A. Algazzar, R. Sathyamurthy, M.K. Ahmed Ali, M.A. Elaziz, et al., Eco-friendly coffee-based colloid for performance augmentation of solar stills, Process Safety and Environmental Protection 136 (2020) 259–267.
[5] Hitesh Panchal, D.K. Patel, Prathik Patel, Theoretical and experimental performance analysis of sandstones and marble pieces as thermal energy storage materials inside solar stills, International Journal of Ambient Energy 39 (3) (2018) 221–229, https://doi.org/10.1080/01430750.2017.1298059.
[6] S.W. Sharshir, Y.M. Ellakany, A.M. Algazzar, A.H. Elsheikh, M.R. Elkadeem, E.M.A. Edreis, et al., A mini review of techniques used to improve the tubular solar still performance for solar water desalination, Process Safety and Environmental Protection 124 (2019) 204–212.
[7] Hitesh Panchal, Effect of Different parameters on double slope solar still productivity. International Journal of Advanced Science and Engineering. 1(2) , 17-21.
[8] S.W. Sharshir, G. Peng, L. Wu, N. Yang, F.A. Essa, A.H. Elsheikh, et al., Enhancing the solar still performance using nanofluids and glass cover cooling: experimental study, Applied Thermal Engineering 113 (2017) 684–693.
[9] Hitesh Panchal, Annual Performance analysis of Double basin solar still with Evacuated tubes, International Journal of Research 4.13 (2017) 889–894.
[10] S.W. Sharshir, G. Peng, A.H. Elsheikh, E.M.A. Edreis, M.A. Eltawil, T. Abdelhamid, et al., Energy and exergy analysis of solar stills with micro/nano particles: a comparative study, Energy Conversion and Management 177 (2018) 363–375.
[11] A.E. Kabeel, R. Sathyamurthy, A.M. Manokar, S.W. Sharshir, F.A. Essa, A.H. Elshiekh, Experimental study on tubular solar still using Graphene Oxide Nano particles in Phase Change Material (NPCM's) for fresh water production, Journal of Energy Storage 28 (2020) 101204.
[12] F.A. Essa, Z.M. Omara, A.S. Abdullah, S. Shanmugan, H. Panchal, A.E. Kabeel, et al., Wall-suspended trays inside stepped distiller with Al2O3/paraffin wax mixture and vapor suction: experimental implementation, Journal of Energy Storage 32 (2020) 102008.
[13] Sandeepsinh Vala, Hitesh Panchal, Bhavesh Kanabar, Comparative performance evaluation of single-slope and pyramid-shaped solar stills: experimental evaluation, International Journal of Ambient Energy 39 (8) (2018) 759–766, https://doi.org/10.1080/01430750.2017.1345012.
[14] Hitesh Panchal, Dinesh Mevada, Kishor Kumar Sadasivuni, F.A. Essa, S. Shanmugan, Mohammand Khalid, Experimental and water quality analysis of solar stills with vertical and inclined fins,Groundwater for Sustainable Development 11 (2020) 100410.
[15] Hitesh Panchal, Kishor Kumar Sadasivuni, M. Suresh, Satyapal Yadav, Shivani Brahmbhatt, Performance analysis of evacuated tubes coupled solar still with double basin solar still and solid fins, International Journal of Ambient Energy 41 (9) (2020) 1031–1037, https://doi.org/10.1080/01430750.2018.1501745.
[16] A.I. Shehata, A.E. Kabeel, M.M. Khairat Dawood, A.M. Elharidi, A. Abd_Elsalam, K. Ramzy, et al., Enhancement of the productivity for single solar still with ultrasonic humidifier combined with evacuated solar collector: an experimental study, Energy Conversion and Management 208 (2020) 112592.
[17] A.H. Abed, H.A. Hoshi, M.H. Jabal, Experimental investigation of modified solar still coupled with high-frequency ultrasonic vaporizer and phase change material capsules, Case Studies in Thermal Engineering 28 (2021) 101531.
[18] A.R.A. Elbar, M.S. Yousef, H. Hassan, Energy, exergy, exergoeconomic and enviroeconomic (4E) evaluation of a new integration of solar still with photovoltaic panel, Journal of Cleaner Production 233 (2019) 665–680.
[19] H. Hassan, M.S. Yousef, M. Fathy, M.S. Ahmed, Assessment of parabolic trough solar collector assisted solar still at various saline water mediums via energy, exergy, exergoeconomic, and enviroeconomic approaches, Renewable Energy 155 (2020) 604–616.
[20] D. Mevada, H. Panchal, K.K. Sadasivuni, Investigation on evacuated tubes coupled solar still with condenser and fins: experimental, exergo-economic and exergo-environment analysis, Case Studies in Thermal Engineering 27 (2021) 101217.
[21] R. Fallahzadeh, L. Aref, N. Gholamiarjenaki, Z. Nonejad, M. Saghi, Experimental investigation of the effect of using water and ethanol as working fluid on the performance of pyramid-shaped solar still integrated with heat pipe solar collector, Solar Energy 207 (2020) 10–21.
[22] T. Long, D. Zheng, Y. Li, S. Liu, J. Lu, D. Shi, et al., Experimental study on liquid desiccant regeneration performance of solar still and natural convective regenerators with/without mixed convection effect generated by solar chimney, Energy 239 (2022) 121919.
[23] N.T. Alwan, S.E. Shcheklein, O.M. Ali, Experimental investigation of modified solar still integrated with solar collector, Case Studies in Thermal Engineering 19 (2020) 100614.
[24] N.T. Alwan, S.E. Shcheklein, O.M. Ali, Evaluation of distilled water quality and production costs from a modified solar still integrated with an outdoor solar water heater, Case Studies in Thermal Engineering 27 (2021) 101216.

[25] L. Mu, X. Xu, T. Williams, C. Debroux, R.C. Gomez, Y.H. Park, et al., Enhancing the performance of a single-basin single-slope solar still by using Fresnel lens: experimental study, Journal of Cleaner Production 239 (2019) 118094.
[26] M.M. Morad, H.A.M. El-Maghawry, K.I. Wasfy, Improving the double slope solar still performance by using flat-plate solar collector and cooling glass cover, Desalination 373 (2015) 1–9.
[27] M. Abu-Arabi, M. Al-harahsheh, M. Ahmad, H. Mousa, Theoretical modeling of a glass -cooled solar still incorporating PCM and coupled to flat plate solar collector, Journal of Energy Storage 29 (2020) 101372.
[28] M. Al-harahsheh, M. Abu-Arabi, H. Mousa, Z. Alzghoul, Solar desalination using solar still enhanced by external solar collector and PCM, Applied Thermal Engineering 128 (2018) 1030–1040.
[29] H. Amiri, M. Aminy, M. Lotfi, B. Jafarbeglo, Energy and exergy analysis of a new solar still composed of parabolic trough collector with built-in solar still, Renewable Energy 163 (2021) 465–479.
[30] S. Arora, H.P. Singh, L. Sahota, M.K. Arora, R. Arya, S. Singh, et al., Performance and cost analysis of photovoltaic thermal (PVT)-compound parabolic concentrator (CPC) collector integrated solar still using CNT-water based nanofluids, Desalination 495 (2020) 114595.
[31] M.A. Eltawil, Z.M. Omara, Enhancing the solar still performance using solar photovoltaic, flat plate collector and hot air, Desalination 349 (2014) 1–9.
[32] G. Sadeghi, S. Nazari, Retrofitting a thermoelectric-based solar still integrated with an evacuated tube collector utilizing an antibacterial-magnetic hybrid nanofluid, Desalination 500 (2021) 114871.
[33] H.S. Mohaisen, J.A. Esfahani, M.B. Ayani, Improvement in the performance and cost of passive solar stills using a finned-wall/built-in condenser: an experimental study, Renewable Energy 168 (2021) 170–180.
[34] M. Feilizadeh, M.R.K. Estahbanati, M. Khorram, M.R. Rahimpour, Experimental investigation of an active thermosyphon solar still with enhanced condenser, Renewable Energy 143 (2019) 328–334.
[35] A.H. Elsheikh, S.W. Sharshir, M. Abd Elaziz, A. Kabeel, W. Guilan, Z. Haiou, Modeling of solar energy systems using artificial neural network: a comprehensive review, Solar Energy 180 (2019) 622–639.
[36] A.F. Mashaly, A.A. Alazba, A.M. Al-Awaadh, M.A. Mattar, Predictive model for assessing and optimizing solar still performance using artificial neural network under hyper arid environment, Solar Energy 118 (2015) 41–58.
[37] F.A. Essa, A.H. Elsheikh, R. Sathyamurthy, A. Muthu Manokar, A.W. Kandeal, S. Shanmugan, et al., Extracting water content from the ambient air in a double-slope half-cylindrical basin solar still using silica gel under Egyptian conditions, Sustainable Energy Technologies and Assessments 39 (2020) 100712.
[38] M. Abd Elaziz, F.A. Essa, A.H. Elsheikh, Utilization of ensemble random vector functional link network for freshwater prediction of active solar stills with nanoparticles, Sustainable Energy Technologies and Assessments 47 (2021) 101405.
[39] N.I. Santos, A.M. Said, D.E. James, N.H. Venkatesh, Modeling solar still production using local weather data and artificial neural networks, Renewable Energy 40 (2012) 71–79.
[40] A.H. Elsheikh, V.P. Katekar, O.L. Muskens, S.S. Deshmukh, M.A. Elaziz, S.M. Dabour, Utilization of LSTM neural network for water production forecasting of a stepped solar still with a corrugated absorber plate, Process Safety and Environmental Protection 148 (2021) 273–282.
[41] A.H. Elsheikh, M. Abd Elaziz, Review on applications of particle swarm optimization in solar energy systems, International Journal of Environmental Science and Technology 16 (2019) 1159–1170.
[42] D. Oliva, M.A. Elaziz, A.H. Elsheikh, A.A. Ewees, A review on meta-heuristics methods for estimating parameters of solar cells, Journal of Power Sources 435 (2019) 126683.
[43] M. Abd Elaziz, A.H. Elsheikh, D. Oliva, L. Abualigah, S. Lu, A.A. Ewees, Advanced Metaheuristic Techniques for Mechanical Design Problems: Review, Archives of Computational Methods in Engineering, 2021.
[44] A.H. Elsheikh, M. Abd Elaziz, A. Vendan, Modeling ultrasonic welding of polymers using an optimized artificial intelligence model using a gradient-based optimizer, Welding in the World (2021).
[45] W.S. AbuShanab, M. Abd Elaziz, E.I. Ghandourah, E.B. Moustafa, A.H. Elsheikh, A new fine-tuned random vector functional link model using Hunger games search optimizer for modeling friction stir welding process of polymeric materials, Journal of Materials Research and Technology 14 (2021) 1482–1493.
[46] A.H. Elsheikh, T. Muthuramalingam, S. Shanmugan, A.M. Mahmoud Ibrahim, B. Ramesh, A.B. Khoshaim, et al., Fine-tuned artificial intelligence model using pigeon optimizer for prediction of residual stresses during turning of Inconel 718, Journal of Materials Research and Technology 15 (2021) 3622–3634.
[47] M.E. Zayed, J. Zhao, W. Li, A.H. Elsheikh, M.A. Elaziz, A hybrid adaptive neuro-fuzzy inference system integrated with equilibrium optimizer algorithm for predicting the energetic performance of solar dish collector, Energy 235 (2021) 121289.
[48] K. Elmaadawy, M.A. Elaziz, A.H. Elsheikh, A. Moawad, B. Liu, S. Lu, Utilization of random vector functional link integrated with manta ray foraging optimization for effluent prediction of wastewater treatment plant, Journal of Environmental Management 298 (2021) 113520.
[49] A.H. Elsheikh, M.A. Elaziz, S.R. Das, T. Muthuramalingam, S. Lu, A new optimized predictive model based on political optimizer for eco-friendly MQL-turning of AISI 4340 alloy with nano-lubricants, Journal of Manufacturing Processes 67 (2021) 562–578.
[50] A.H. Elsheikh, M. Abd Elaziz, B. Ramesh, M. Egiza, M.A.A. Al-qaness, Modeling of drilling process of GFRP composite using a hybrid random vector functional link network/parasitism-predation algorithm, Journal of Materials Research and Technology 14 (2021) 298–311.
[51] F.A. Essa, M. Abd Elaziz, A.H. Elsheikh, Prediction of power consumption and water productivity of seawater greenhouse system using random vector functional link network integrated with artificial ecosystem-based optimization, Process Safety and Environmental Protection 144 (2020) 322–329.
[52] A.B. Khoshaim, A.H. Elsheikh, E.B. Moustafa, M. Basha, A.O. Mosleh, Prediction of residual stresses in turning of pure iron using artificial intelligence-based methods, Journal of Materials Research and Technology 11 (2021) 2181–2194.
[53] A.H. Elsheikh, T.A. Shehabeldeen, J. Zhou, E. Showaib, M. Abd Elaziz, Prediction of laser cutting parameters for polymethylmethacrylate sheets using random vector functional link network integrated with equilibrium optimizer, Journal of Intelligent Manufacturing 32 (2021) 1377–1388.
[54] F.A. Essa, M. Abd Elaziz, A.H. Elsheikh, An enhanced productivity prediction model of active solar still using artificial neural network and Harris Hawks optimizer, Applied Thermal Engineering 170 (2020) 115020.
[55] M. Bahiraei, S. Nazari, H. Safarzadeh, Modeling of energy efficiency for a solar still fitted with thermoelectric modules by ANFIS and PSO-enhanced neural network: a nanofluid application, Powder Technology 385 (2021) 185–198.
[56] T.A. Shehabeldeen, M.A. Elaziz, A.H. Elsheikh, J. Zhou, Modeling of friction stir welding process using adaptive neuro-fuzzy inference system integrated with harris hawks optimizer, Journal of Materials Research and Technology 8 (2019) 5882–5892.
[57] M. Abd Elaziz, T.A. Shehabeldeen, A.H. Elsheikh, J. Zhou, A.A. Ewees, M.A.A. Al-qaness, Utilization of Random Vector Functional Link integrated with Marine Predators Algorithm for tensile behavior prediction of dissimilar friction stir welded aluminum alloy joints, Journal of Materials Research and Technology 9 (2020) 11370–11381.
[58] A.H. Elsheikh, A.I. Saba, M.A. Elaziz, S. Lu, S. Shanmugan, T. Muthuramalingam, et al., Deep learning-based forecasting model for COVID-19 outbreak in Saudi Arabia, Process Safety and Environmental Protection 149 (2021) 223–233.
[59] L. Ni, D. Wang, V.P. Singh, J. Wu, Y. Wang, Y. Tao, et al., Streamflow and rainfall forecasting by two long short-term memory-based models, Journal of Hydrology 583 (2020) 124296.
[60] S. Mirjalili, Moth-flame optimization algorithm: a novel nature-inspired heuristic paradigm, Knowledge-based systems 89 (2015) 228–249.
[61] A.H. Elsheikh, S.W. Sharshir, M. Abd Elaziz, A.E. Kabeel, W. Guilan, Z. Haiou, Modeling of solar energy systems using artificial neural network: a comprehensive review, Solar Energy 180 (2019) 622–639.
[62] Hitesh Panchal, Nikunj Patel, Hemin Thakkar, Various techniques for improvement in distillate output from active solar still: a review, International Journal of Ambient Energy 38 (2) (2017) 209–222, https://doi.org/10.1080/01430750.2015.1076518.
[63] H. Panchal, K.K. Sadasivuni, S. Shanmugan, N. Pandya, Performance analysis of waste brick magnesia as a storage material in a solar still, Heat Transfer 50 (2021) 1799–1811, https://doi.org/10.1002/htj.21956.